CORROSION SCIENCE AND TECHNOLOGY, Vol.17, No.5(2018), pp.249~256
[Review Paper]
pISSN: 1598-6462 / eISSN: 2288-6524
DOI: https://doi.org/10.14773/cst.2018.17.5.249

Investigation of Sweet and Sour Corrosion of Mild Steel in Oilfield Environment by Polarization, Impedance, XRD and SEM Studies

Subir Paul[1,†] and Bikramjit Kundu[2]

[1]*Professor, Dept of Metallurgical and Material Engineering, Jadavpur University Kolkata, India*
[2]*Engineer, Dept of Metallurgical and Material Engineering, Jadavpur University Kolkata, India*

(Received September 07, 2018; Revised October 05, 2018; Accepted October 08, 2018)

Metallic structures in the oil and gas production undergo severe degradation due to sweet and sour corrosion caused by the presence of CO_2 and H_2S in the fluid environment. The corrosion behavior of 304 austenitic stainless was investigated in the presence of varying concentrations of CO_2 or H_2S and CO_2 + H_2S to understand the effect of the parameters either individually or in combination. Potentiodynamic polarization study revealed that a small amount of CO_2 aided in the formation of calcareous deposit of protective layer on passive film of 304 steel, while increase in CO_2 concentration ruptured the layer resulting in sweet corrosion. The presence of S^{2-} damaged the passive and protective layer of the steel and higher levels increased the degradation rate. Electrochemical impedance studies revealed lower polarization resistance and impedance at higher concentration of CO_2 or H_2S, supporting the outcomes of polarization study. XRD analysis revealed different types of iron carbides and iron sulphides corresponding to sweet and sour corrosion as the corrosion products, respectively. SEM analysis revealed the presence of uniform, localized and sulphide cracking in sour corrosion and general corrosion with protective carbide layer amid for sweet corrosion.

Keywords: *Oil field corrosion, mild steel, polarization, impedance spectroscopy, electron microscopy*

1. Introduction

Sweet and sour corrosion of steel structure in the well and transportation pipeline in the oil and gas system is a major problem of equipments and monetary loss for oil and gas industries. To combat this corrosion effect, the oil and gas industries use expensive high corrosion resistant materials and other protective methods. The oil production unit is in the marine seawater environment, which itself is very corrosive due to presence of Cl- ,SO_4^{2-}, HCO_3^- , CO_3^{2-} and the dissolved oxygen. The sweet corrosion is caused by the presence of CO_2 and the sour corrosion by the presence of H_2S in the oil and gas marine environment. They produce corrosion species HCO_3^-, CO_3^{2-}, S^{-2} in addition to Cl^-, contributing to huge degradation rate in oil field sea water. The concentration of these species also vary depending on the geographical location of the structures across the different ocean and sea water as well as along the depth [1]. The pH of sea water is normally in the range of neutral to slightly alkaline, but local acidity develops, due to corrosion products as well as crude petroleum products, lowering the pH to less than 4. Temperature is also not fixed but varies due to seasonal change and geographical location of an oil field site. Each and every parameter has direct influence on the degradation rate of the submerzed structures. Chloride ion aggravates the degradation of materials in aqueous environment [2-8]. It helps in breaking passive oxide layer, leading to localized corrosion of crevice and pitting corrosion. pH has a variable effect on corrosion. Both very low and high pH are detrimental to corrosion.

Sweet corrosion is a significant problem in the oil and gas production and transportation (transmission and distribution) systems. Downhole CO_2 corrosion in the production systems has received significant attention due to the high CO_2 content in the oil and gas production fluids that can cause significant failures of the pipes in wells. Sour corrosion is caused by salts and sulfide compounds dissolved in crude oil. These provoke the formation of a corrosive aqueous solution whose chemical composition involves the presence of both hydrochloric acid (HCI) and hydrogen sulfide (H_2S). Previous researches [9-11] have shown that H_2S had a remarkable acceleration effect on both the anodic iron dissolution and the cathodic evolution

†Corresponding author: spmet4@gmail.com

Table 1 Composition of artificial sea water (ASTM D1141-2003)

NaCl	Na_2SO_4	$NaHCO_3$	KCl	KBr,	$MgCl_2.6H_2O$	$CaCl_2.6H_2O$	$MgCl_2.6H_2O$	$SrCl_2.6H_2O$	H_3BO_3
Concentration in gm/liter									
23.47	3.917	0.192	0.664	0.096	10.61	1.469	10.61	0.04	0.026

In general the influence of any of the these parameters is independently known. But conjoint effects of the above mentioned multiple parameters and the interrelationship among the variables on corrosion rate are complex and not known. The influence of so many factors on the corrosion rate, necessitates modeling and simulation of corrosion process. Corrosion models [12-20] have been developed by by Artificial neural network (ANN), Genetic algorithm (GA) and Finite element method (FEM) to study the effect of these parameters and predict the corrosion rate. Mechanisms of the corrosion process are better understood from the modeling and simulation and right protective methods can be applied [21].

304 austenitic stainless steel which is corrosion resistant due to the formation of passive film is also prone to corrosion in such environment with breakdown of passive film, leading to localized and general corrosion.

In the present investigation, corrosion behavior of 304 stainless steel has been studied in synthetically produced sea water having above mentioned ions. Potentiodynamic studies have been extensively carried out by varying each of these parameters and computing corrosion potential and corrosion current.

Electrochemical AC impedance spectroscopy studies were also carried out for better understanding of electrochemical effects of corrosive species on electrical phenomenon occurring at metal-solution interface. The corroded substrates were characterized by XRD. The morphology of the uncorroded and corroded surface were investigated by scanning electron microscopy.

2. Experimental Methods

The test specimen was 1 cm x 1 cm of low carbon steel Experiments were conducted in 3.5% NaCl solution (NACE solution). Sweet Corrosion of the sample was studied by bubbling CO_2 through the artificially sea water solution (Table 1). CO_2 was generated from an apparatus with the the following reaction:

$$CaCO_3 + 2HCl = CaCl_2 + CO_2 + H_2O$$

The time of bubbling was noted and pH of the solution was checked. The CO_2 bubbled would form carbonic acid that would contribute to the lowering of pH. The amount of CO_2 ranged from 3.5 ppm-170 ppm (average sea water composition is reported having 90 ppm)

Sour Corrosion of the sample was studied by adding right amount of Na_2S in the artificially prepared sea water solution. This too liberates S^{2-} ions and has similar affects to that of H_2S passing. The S^{2-} concentration was kept between 14 gm/l and 24 gm/l.

2.1 Polarization Studies

Electrochemical measurements were conducted as ASTM standards [22,23], using Gamry Potentiostat instrument coupled with Echem analyst software, controlled by a personal computer, in a conventional three-electrode cell systems. The working electrode was carbon steel, the counter electrode was graphite, and a saturated calomel electrode (SCE) acted as the reference electrode. Experiments were performed in different concentrations of Cl^-, SO_4^{2-}, CO_2 and S^{2-} solutions, at preselected pH and temperature, to determine the corrosion potential Ecorr and corrosion current $i$corr. The potential was scanned between −1.5 V and 1 V at a scan rate of 1 mV/s

2.2 Electrochemical Impedance Spectroscopy (EIS)

The experimental arrangement was the same as that of polarization studies. The electrochemical cell was connected to an impedance analyzer (EIS300 controlled by Echem analyst software) for electrochemical impedance spectroscopy. The electrochemical impedance spectrawere obtained at frequencies between 300 kHz and 0.01Hz.The amplitude of the sinusoidal wave was 10mV.The following results and information are obtained from the EIS experiments: Polarization resistance

($R\,p$), electrolyte resistance ($R\,u$), double layer capacitance (Cdl), capacitive load or constant phase element, CPE(Y), and α which is defined from the capacitive impedance equation $Z = 1/C(jw)^{-\alpha}$.

Capacitors in EIS experiments often do not behave ideally. Instead, they act like a constant phase element (CPE). The exponent $\alpha = 1$ for pure capacitance. For a constant phase element, the exponent α is less than one. The “double layer capacitor” on real cells often behaves like a CPE instead of like a pure capacitor

Table 2 Computed Corrosion Data of Sweet and Sour corrosion

System	Concentration	pH	Temperature °C	E_{corr} volt Vs SCE	I_{corr} mA/cm^2
Sweet Corrosion	CO_2 0 ppm	7.0	25	-0.53	0.050
Sweet Corrosion	CO_2 20 ppm	7.0	25	-0.57	0.023
Sweet Corrosion	CO_2 50 ppm	7.0	25	-0.68	0.718
Sweet Corrosion	CO_2 100 ppm	7.0	25	-0.86	0.828
Sweet Corrosion	CO_2 50 ppm	4	25	-0.76	0.832
Sweet Corrosion	CO_2 50 ppm	7.0	25	-0.57	0.231
Sweet Corrosion	CO_2 50 ppm	9.0	25	-0.77	0.091
Sweet Corrosion	CO_2 50 ppm	7.0	25	-0.53	0.712
Sweet Corrosion	CO_2 50 ppm	7.0	50	-0.87	0.005
Sweet Corrosion	CO_2 50 ppm	7.0	80	-0.77	0.78
System	**Concentration**	**pH**	**Temperature °C**	**E_{corr} volt Vs SCE**	**I_{corr} mA/cm^2**
Sour Corrosion	S^{2-} 2 gm/l	7.0	25	-0.58	0.006
Sour Corrosion	S^{2-} 14 gm/l	7.0	25	-0.72	0.09
Sour Corrosion	S^{2-} 20 gm/l	7.0	25	-0.68	1.12
Sour Corrosion	S^{2-} 14 gm/l	4.0	25	-0.64	0.98
Sour Corrosion	S^{2-} 14 gm/l	7.0	25	-0.57	0.08
Sour Corrosion	S^{2-} 14 gm/l	9.0	25	-0.52	0.004
Sour Corrosion	S^{2-} 14 gm/l	7.0	25	-0.58	0.006
Sour Corrosion	S^{2-} 14 gm/l	7.0	50	-0.63	0.89
Sour Corrosion	S^{2-} 14 gm/l	7.0	80	-0.72	1.03

2.3 X-Ray Diffraction (XRD) Analysis

The X-ray diffraction technique is used to define the crystalline structure and the crystalline phases. This test was done using a Rigaku Ultima III X-Ray Diffractometer for recording the diffraction traces of the samples with monochromatized Cu Kα radiation, at room temperature; the scan region (2θ) ranged from 10^0 to 100^0 at a scan rate of 5^0 min^{-1}.

Microstructures of the corroded specimens were observed under Leica Optical Microscope.

2.4 Scanning Electron Microscope (SEM) Morphology

The electron micrographs were studied by SEM with accelerating voltage 30 kV, magnification up to 300,000x, and resolution of 3.5 nm. The images of the corroded samples were photographed at low and high magnification

3. Results

The effects of variation of concentration of CO_2 and S^{-2} on degradation behavior of carbon steel were studied by Potentiostatic polarization and the various electrical properties at the metal solution by Electrochemical impedance spectroscopy (EIS). The presence of different compounds on corroded surface was detected by XRD. The morphology of the degraded surfaces is characterized by SEM.

3.1 Polarization Studies

Fig. 1 shows the polarization curves of steel in sweater with variation of CO_2 concentration. It is found that increase in CO_2 concentration shifts the curves to the right, indicating an increase in corrosion rate. But the corrosion rate is found to be the minimum at 20 ppm CO_2 concentration and it is less than the values at 0 ppm concentration. Variation of pH in the oil field environment may influence the rate of sweet corrosion (Fig. 2). It is seen that the corrosion rate increases with higher acidity

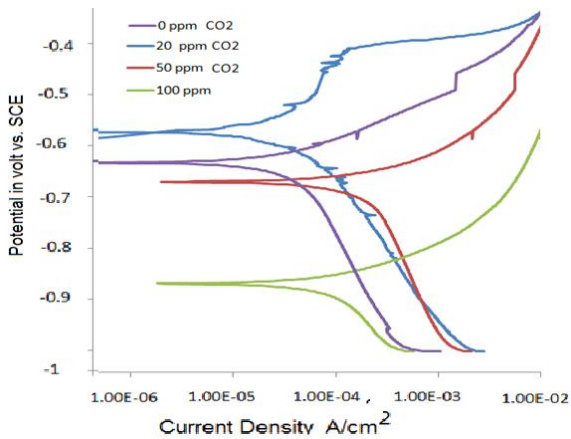

Fig. 1 Potentiodynamic polarization comparison of CO_2 corrosion at different concentration.

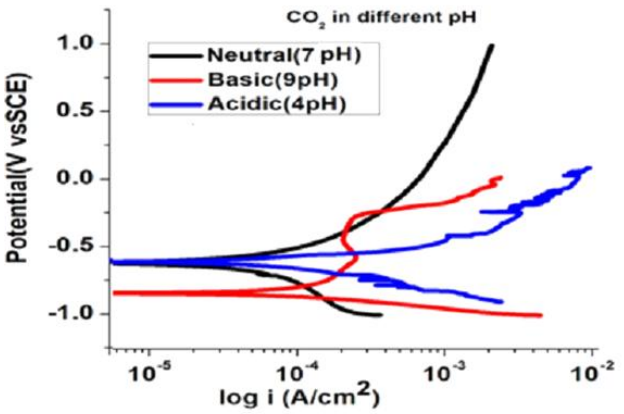

Fig. 2 Potentiodynamic polarization comparison of 50 ppm CO_2 corrosion at different pH.

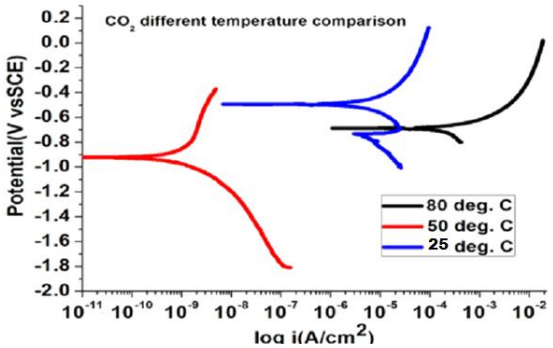

Fig. 3 Potentiodynamic polarization comparison of CO_2 corrosion at different temperature.

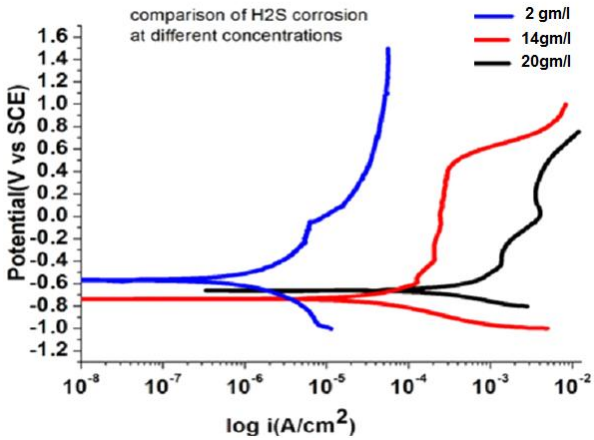

Fig. 4 Potentiodynamic polarization comparison of H_2S corrosion at different concentration.

or alkalinity compared to that under neural pH. This is due to breakdown of protective carbonate layer. The effect is more in acidic region compared to other. Temperature in ocean oil field environment changes due to exothermic reactions in the petroleum products as well as geo-

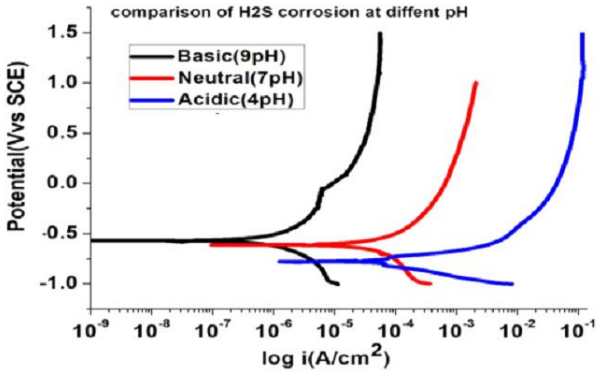

Fig. 5 Potentiodynamic polarization comparison of H_2S corrosion at different pH.

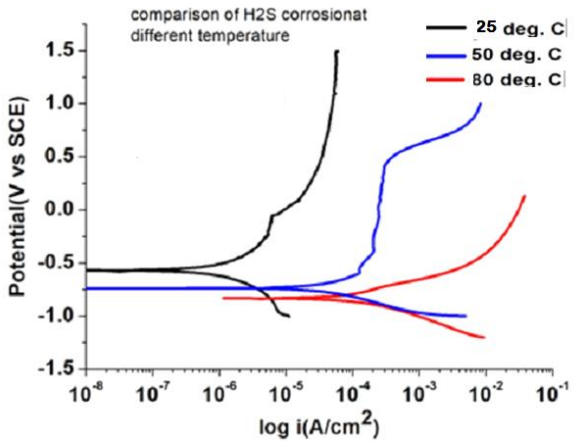

Fig. 6 Potentiodynamic polarization comparison of H_2S corrosion at different temperature.

graphical location and seasonal change. The effect of temperature on sweet corrosion (Fig. 3) is having dual effect. Normally increase in temperature increases the corrosion rate as the diffusion of corrosion species is faster, the fact decreases the concentration polarization. But on the other hand, increases in temperature decreases the dissolved gases, O_2 and CO_2 which decrease the corrosion

Fig. 5 and 6 illustrate the effects of pH and temperature change, on sour corrosion, keeping H_2S fixed at 0.5 gm/l. It is seen that sour corrosion decreases under alkaline condition (Fig. 5) and becomes very high in acidic condition. Temperature is found to accelerate sour corrosion rate (Fig. 6). Table 2 illustrates the effect of various parameters on sweet and sour corrosion rates.

3.2 Electrochemical Impedance Study (EIS)

All the above studies show that both sweet and sour corrosion aggravate steel. The effect of sour corrosion is much damaging to steel compared to sweet corrosion. Now for better understanding of the fundamental aspects

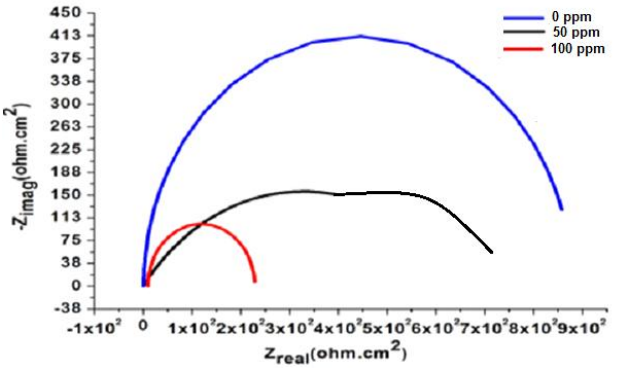

Fig. 7 Nyquist Plot of EIS data with variation of CO_2 concentration.

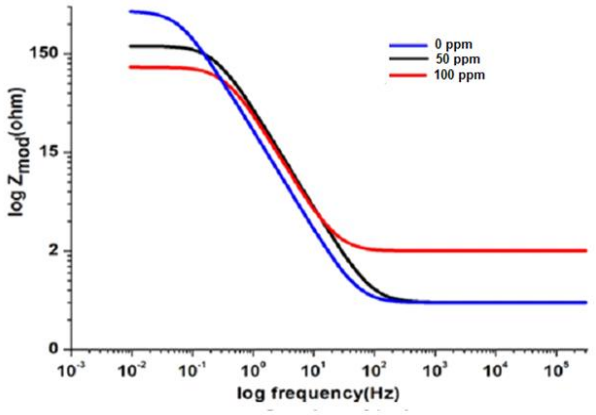

Fig. 8 Bode Plot of EIS data with variation of CO_2 concentration.

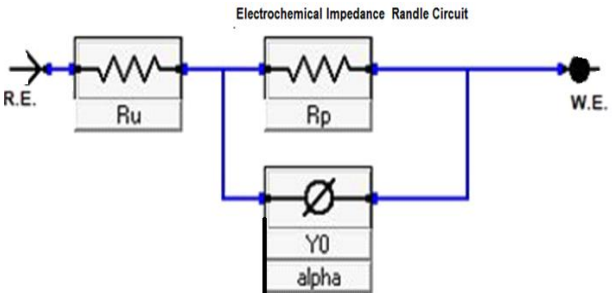

Fig. 9 Model circuit of EIS.

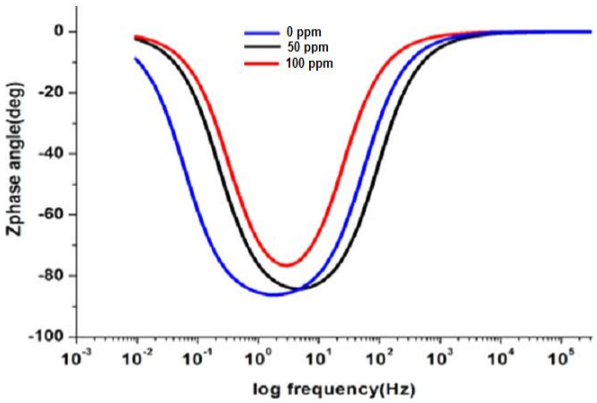

Fig. 10 Bode Plot of EIS data phase angle with variation of CO_2 concentration.

of electrochemical science of sweet and sour corrosion,, . EIS study helps to understand the electrochemical phenomena occurring at the metal-seawater interface, effect of ions and computed R-L-C circuit. In general, the interface consists of layer of (+ve) charge and a layer of (-ve) charge which is called electrical double layer, which produce a capacitance (C_{dl}) or pseudo-capacitance (Y_0). The degree of capacitance is know from the parameter α. If α is close to, the capacitance is pure, else it is a pseudo-capacitance. In addition, there are resistance load for polarization resistance (Rp), solution resistance(Rs). The phenomenon can be interpreted by Nyquist and Bode plot, which are depicted and discussed in the following section for various corrosion effects.

EIS study is carried out. Fig. 7 illustrates electrochemical impedance study by a Nyquist of the steel in sweet corrosive environment with the variation of concentration of CO_2. Nyquist plots show semi circle. The diameter of the semicircle indicates the polarization resistance, R_p. It is interesting to see this diameter decreases with increase in CO_2 concentration, that is polarization resistance becomes less. In the bode plot of the same study (Fig. 8), the impedance Z is of high value for the case of minimum CO_2. It shows both Impedance and resistance become high for the sweet corrosion the least CO_2 concentration. The EIs data fit the simple Randle circuit (Fig. 9) with a capacitance (Y_0)parallel to polarization resistance (R_p)and both in series with solution resistance (R_u). The computed EIs parameters are shown in Table 2. The phase angle shifts (Fig. 10) towards -90 degree, indicating presence of capacitance or pseudo capacitance in the RLC circuit.

EIS studies for sour corrosion are similarly shown in Fig.s 11,12 and 13 for Nyquist plot, Bode plot and phase angle shifts respectively. EIS data in sour corrosion also match the model circuit in Fig. 9 and the computed EIS parameters are given in table 3. Bode plot reflects the diameter of the semi circle decreases with increasing in sulphide concentration (Fig. 11), indication polarization resistance is decreasing and the impedance too is getting lowered (Fig. 12) in the bode plot.

3.3 XRD Analysis of Corrosion products

Fig.s 14 and 15 show X ray diffraction graphs of the corroded steel in sweet corrosion and sour corrosion

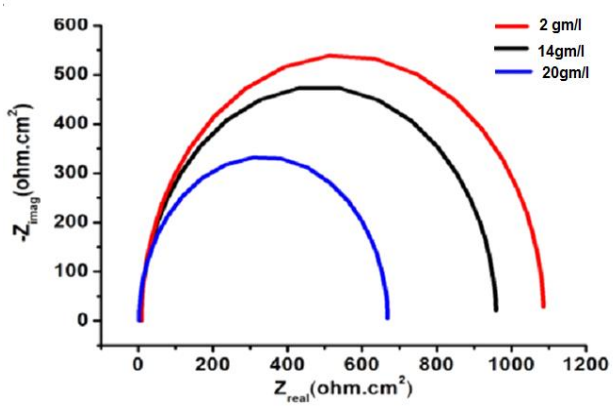

Fig. 11 Nyquist Plot of EIS data with variation of H_2S concentration.

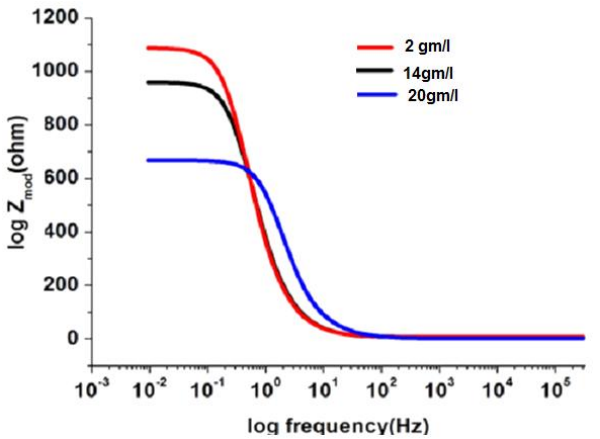

Fig. 12 Bode Plot of EIS data with variation of H_2S concentration.

Table 3 Computed EIS Data for sweet corrosion of steel in seawater (Fig. 7, 8)

CO_2 concentration (ppm)	Rp (ohm.cm2)	Y_0 µF	alpha
0	850	110	0.84
50	550	143	0.70
100	250	178	0.60

Table 4 Computed EIS Data for sour corrosion of steel in seawater (Fig. 10, 11)

Sulphide Concentration gm/l	Rp(ohm.cm2)	Y_0 µF	alpha
2	1200	121	.80
14	1000	139	.74
20	620	175	.66

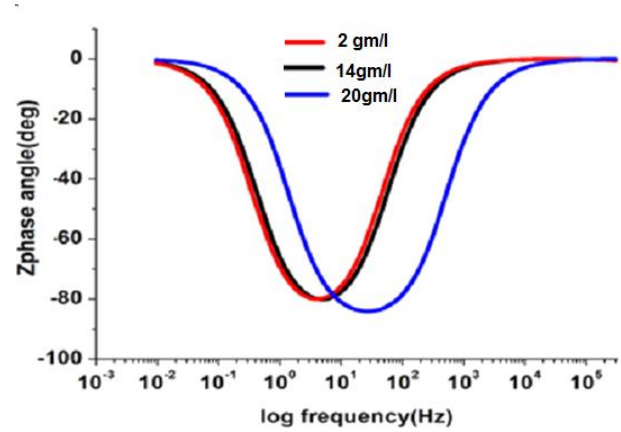

Fig. 13 Bode Plot of EIS data phase angle with variation of H_2S concentration.

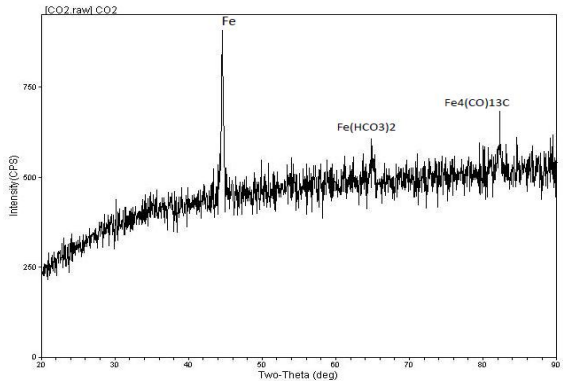

Fig. 14 XRD analysis of corroded steel sample in 3.5% NaCl solution + 20. ppm CO_2.

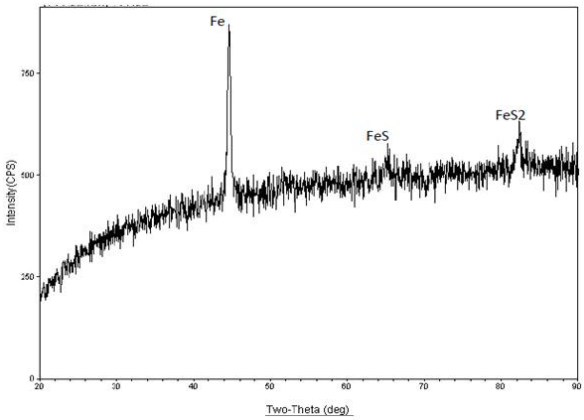

Fig. 15 XRD analysis of corroded steel sample in 3.5% NaCl solution + 14 g/l H_2S.

respectively. It shows the corroded products of sweet corrosion: $Fe_4(CO)_{13}C$, $Fe(HCO_3)_2$ and sour corrosion: Mackinawite (FeS) and FeS_2.

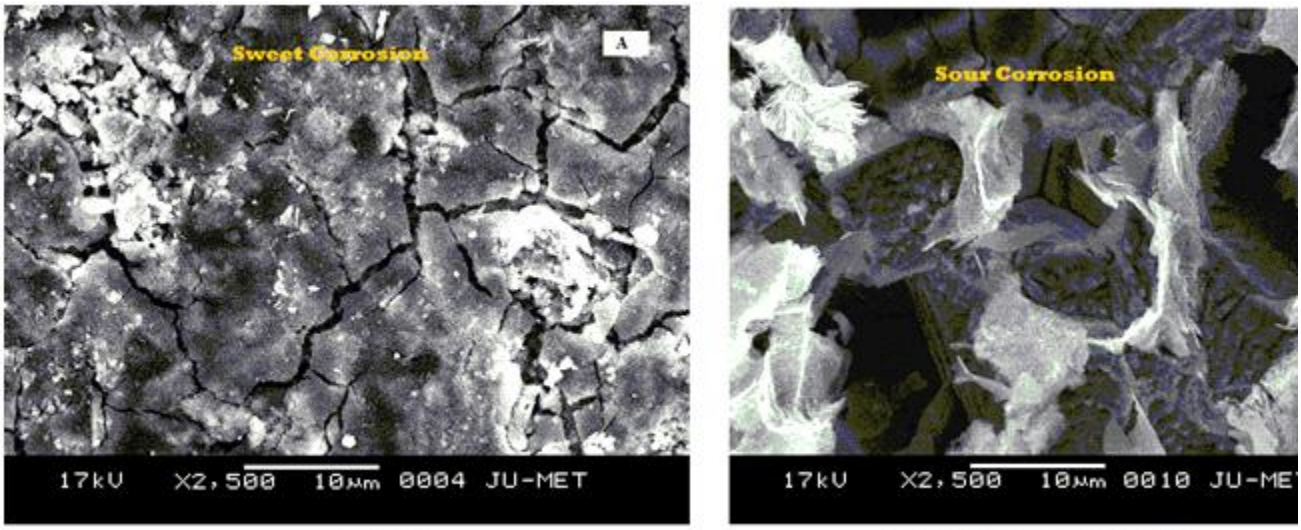

Fig. 16 SEM images of sweet (A) and sour Corrosion (B) in 3.5% NaCl solution + 50 ppm CO_2 (A) in and 3.5% NaCl solution + 10 g/l H_2S (B).

3.5 SEM Images

The morphology of the sweet and sour corroded surface observed under scanning electron microscope is shown in Fig. 16. The sweet corrosion (Fig. 16A) shows uniform and some localized damage with presence of protective carbonate layer (white part) at some areas. It was found in the polarization study of sweet corrosion that corrosion rate at about 20 ppm CO_2 presence is less than zero CO_2. This is due to the formation of calcareous deposit of carbonate layer. This is indicated by the presence of $Fe(HCO_3)_2$ phase in XRD study (Fig. 14). In sour corrosion (Fig. 16B), the black corrosion products (FeSx) formed on the steel surface in the H_2S-containing solutions could be observed. The damage of the sour corrosion is severe from pitting to sulphide cracking. The images support the corrosion products formed in the XRD study in Fig.s 15.

4. Discussion

The main electrochemical anodic and cathodic reactions for the corrosion of carbon steel in aqueous oilfields environments in presences of the ions are as follows

$2Fe = 2Fe^{++} + 4e$ Anodic
$2H_2O + O_2 + 4e = 4OH^-$ Cathodic
$2Fe + 2H_2O + O_2 = 2Fe(OH)_2$ (Rust) Overall

4.1 Sweet Corrosion

Carbonate ion is produced from CO_2 gas as explained in the following reactions.

$CO_2 + H_2O = H_2CO_3$
$H_2CO_3 = HCO^{3-} + H^+$
$2HCO_3^- + 2e- = H_2 + 2CO_3^{2-}$

So it produces acidity H^+, carbonate CO_3^{2-} and bicarbonate HCO^{3-}. Acidity increases the corrosion rate, HCO^{3-} on hydrolysis produces H^+ and hence it also aggravates the degradation of passive layer. But CO_3^{2-} produces a protective layer on steel surface by the following reaction and hence passivity is strengthened and steel is protected. Thus a small concentration of CO_2 is helpful in protecting passivity layer.

$Fe^{2+} + CO_3^{2-} = FeCO_3$

4.2 Sour Corrosion

The effect of S^{2-} variation on the corrosion rate of steel is shown in Fig. 4. It is seen that the corrosion rate increase severely with increase in S^{2-} concentration. Sulphide is a notorious ion present in oil and gas system which severely attacks the steel. The nature of the curve shows somewhat passivity and passivity breakdown, leading to localized corrosion. Steel exhibits passivity at pH 9 and it acts as protective layer in preventing sour corrosion while under acidic condition this passive layers breaks and S^{-2} can penetrate the steel surface , causing localized to general corrosion. Temperature is found to accelerate sour corrosion rate (Fig. 6) due to the face that

diffusion rate of S^{-2} ions becomes faster with increase in temperature from the bulk of the solution to the metal-solution interface and so the concentration of the ions is always high at the interface.

The deterioration of metal due to contact with S^{-2} (H_2S) and moisture is sour corrosion. The general equation of sour corrosion can be expressed as follows [21]:

$$S^{-2} + 2H^{+} = H_2S\ (aq) \qquad E= 0.097\ V\ vs:\ SCE$$

Hydrogen sulphide will then dissociate to produce proton and bisulphide as described [22] by following equations.

$$H_2S\ (aq) = H^{+} + HS^{-} \qquad K= 9.1\ X\ 10^{-8}$$
$$HS^{-}\ H^{+} + S^{-2} \qquad K= 9.1\ X\ 10^{-12}$$

This reaction scheme shows that presence of hydrogen sulfide can contribute to the concentration of sulfide at the surface by dissociation rather than charge exchange with the surface. The sulfide concentration at the surface is, therefore, dependent on the concentration of aqueous hydrogen sulfide in the electrolyte as well as the reduction processes of sulfate.

H_2S exhibited the different role on anodic process of carbon steel depending on the pH value in the solutions. The local super saturation of FeS_x could be formed on the carbon steel surface via the following reaction, with the nucleation and growth of one or more of the iron sulfide, mackinawite.

$$H_2S + Fe + H_2O \rightarrow FeS_x + 2H + H_2O$$

5. Conclusions

Carbon steel gets severely corroded by sweet and sour corrosion due to presence of CO_2 and H_2S environment in the oil field. Increasing the concentration of these species strong influence in braking down the protective layer and aggravation the degradation process. High corrosion rate is associated by low polarization resistance and impedance. Metallic carbide and sulphide are the corrosion products as detected by XRD. Morphology of the corroded surface under SEM show uniform corrosion with carbonate protective layer in sweet corrosion and localized corrosion with sulphide cracking in sour corrosion.

References

1. Dechema, *Handbook of Corrosion, Weinheim*: VCH Publishers, Vol. 11, NY, USA (1992).
2. J. Robert and M. E. Robert, The changing Topography of Corroded mild Steel Surface in Seawater, *Corros. Sci.*, **49**, 2270 (2007).
3. Ch. Barchiche, C. Deslouis, O. Gil, S. Joiret, Ph. Refait, and B. Tribollet, *Electrochim. Acta*, **54**, 3580 (2009).
4. M. A. Deyab and S. T. Keera, *Egypt. J. Petrol*., **21**, 31 (2012).
5. S. Peter, S. Roy, S. David, M. Stephen, P. David, and L. John, *Chem. Eng. Sci*., **66**, 5775 (2011).
6. R. E. Melchers, *Corrosion,* **59**, 335 (2003).
7. M. L. Free, W. Wang, and D. Y. Ryu, *Corrosion*, **60**, 837 (2004).
8. S. Nesic, *Corros. Sci*., **49**, 4308 (2007).
9. H. H. Huang, W. T. Tsai, and J. T. Lee, *Electrochim. Acta*, **41**, 1191 (1996).
10. J. Tang, Y. Shao, J. Guo, T. Zhang, G. Meng, and F. Wang, *Corros. Sci*., **52**, 2050 (2010).
11. P. Smith and D. Swailes, *Chem. Eng. Sci.,* **66**, 5775 (2011).
12. Subir Paul, Modeling to study the effect of environmental parameters on corrosion of mild steel in seawater using neural network, *ISRN Metallurgy*, Article ID 487351, 6 (2012).
13. S. Paul, *J. Mater. Eng. Perform*., **20**, 325 (2011).
14. S. Paul, *Can. Metall. Quart.*, **45**, 99 (2010).
15. S. Paul, S. K Guchhait, and K. Goswami, *Innovat. Corros. Mater. Sci.*, **4**, 127 (2014).
16. S. Paul and I. Biswas, *Innovat. Corros. Mater. Sci.*, ***5,*** 10 (2015).
17. S. Paul*J. Mater. Eng. Perform.*, **20**, 325 (2012).
18. S. Paul, *Res. Rev. Electrochem.*, **5**, 77 (2014).
19. S. Paul, *Innovat. Corros. Mater. Sci.*, **4**, 127 (2014).
20. S. Paul, *J. Comput. Intel. Electr Sys.*, **l3**, 1 (2014).
21. S. Paul, *Corrosion and Protection of Materials: Understanding and Application,* Amazon Book Store (2017). https://www.amazon.in/dp/B074DQSR96
22. ASTM G 5, Potentiostatic and Potentiodynamic Anodic Polarization Measurements (1993).
23. ASTM G 59, Polarization Resistance Measurements (1992).